A Metal–Organic Framework with Cooperative Phosphines That Permit Post-Synthetic Installation of Open Metal Sites

Samuel G. Dunning, Gianne Nandra, Adam D. Conn, Wenrui Chai, R. Eric Sikma, Ji Sun Lee, Pranaw Kunal, Joseph E. Reynolds III, Jong-San Chang, Alexander Steiner, Graeme Henkelman, and Simon M. Humphrey*

Abstract: PCM-101 is a phosphine coordination material comprised of tris(p-carboxylato)triphenylphosphine and secondary pillaring groups coordinated to $[M_3(OH)]^{5+}$ nodes (M = Co, Ni). PCM-101 has a unique topology in which R_3P: sites are arranged directly trans to one another, with a P···P separation distance dictated by the pillars. Post-synthetic coordination of soft metals to the P: sites proceeds at room temperature to provide X-ray quality crystals that permit full structural resolution. Addition of AuCl groups forces a large distortion of the parent framework. In contrast, CuBr undergoes insertion directly between the trans-P sites to form dimers that mimic solution-phase complexes, but that are geometrically strained due to steric pressure exerted by the MOF scaffold. The metalated materials are active in heterogeneous hydroaddition catalysis under mild conditions, yielding different major products compared to their molecular counterparts.

Metal–organic frameworks (MOFs) are an attractive platform for the synthesis of new types of heterogeneous catalysts.[1] Unlike amorphous catalysts prepared by deposition of molecular species onto support substrates (for example, aluminosilicates), the crystalline nature of MOFs allows for incorporation of structurally well-defined metal sites by design. The microporous nature of MOFs could also provide size- and chemo-selective gating between reagents and the catalyst sites inside the pores, while also providing a large volumetric density of active sites.[2]

Demonstrations of these principles are relatively few in number.[3] The three most common synthetic strategies employed to access such materials are as follows. The first is by the generation of open metal sites in a pre-formed MOF via removal of labile, coordinated solvent molecules.[4] This method is simple, but dependent on the structure of a given framework and generates a limited range of open metal sites. The second is by the use of pre-functionalized building blocks to assemble MOFs with chemical handles that permit post-synthetic modification. This method is more widely applicable for the coordination of metals, or via organic reactions to install secondary metal coordination sites.[5] A downfall of this approach is that such modifications can cause loss of crystallinity, preventing full structural determination of the products. The third is by the use of pre-formed, molecular complexes as MOF building blocks.[6] This direct method can provide crystalline products that permit full structural elucidation by X-ray diffraction, but precursor complexes can undergo decomposition (for example, leaching) under MOF-forming conditions. As such, chelated complexes are preferred, but their preparation can be arduous and low-yielding.

We have recently concentrated on the synthesis of phosphine coordination materials (PCMs) using organophosphines as MOF building blocks, since they are ubiquitous in organometallic chemistry.[7] Our earlier research using mono-phosphines (R_3P) to prepare PCMs gave limited scope for post-synthetic addition of reactive metal species via route 2 (above), because it is difficult to assemble materials with two or more P: sites that permit co-operative metal chelation. Instead, we explored the use of pre-formed phosphine coordination complexes decorated with ancillary carboxylic acids (namely, approach 3). We showed that Pd^{II} or Pt^{II} complexes of carboxylated bis(phosphines)[6a] and PCP-pincers[6b,c] could be used to prepare porous PCMs with unique solid-state reactivity. However, the multi-step routes to prepare the precursors are complicated and large quantities are usually required in the search for optimal MOF-forming conditions.

In the quest to identify a simpler, more versatile and scalable method, we attempted to merge the former two strategies by using monophosphines to spontaneously assemble PCMs with bidentate (P_2) coordination sites. The specific intention was to fuse 2D phosphine-decorated bilayers[8] into 3D arrays, such that the P: sites were arranged directly *trans* to each other. This goal was recently achieved using pillaring organic groups.

PCM-101 is a 3D microporous MOF based on coordination of tris(p-carboxylato)triphenylphosphine (P{C_6H_4-4-

[*] S. G. Dunning, G. Nandra, A. D. Conn, W. Chai, R. E. Sikma, P. Kunal, J. E. Reynolds III, G. Henkelman, S. M. Humphrey
Department of Chemistry, The University of Texas at Austin
105 E 24th Street A5300, Welch Hall 2.204, Austin, TX 78712-1224 (USA)
E-mail: smh@utexas.edu

J. S. Lee, J.-S. Chang
Research Center for Nanocatalysts
Korea Research Institute of Chemical Technology
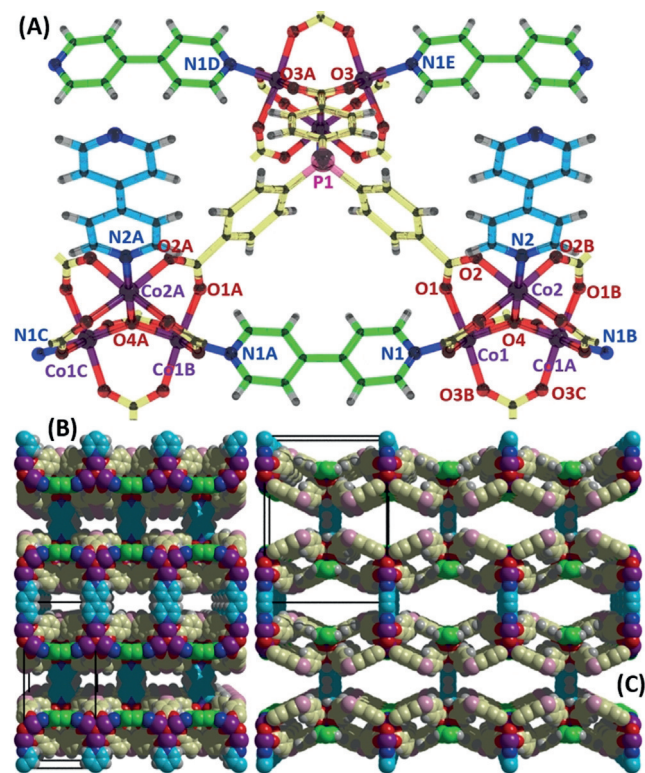P.O. Box 107, Yusung, Daejeon 305-600 (Korea)

J.-S. Chang
Department of Chemistry, Sungkyunkwan University
Suwon 440-476 (Korea)

A. Steiner
Department of Chemistry, University of Liverpool
Crown St., Liverpool L69 7ZD (UK)

Supporting information (materials and methods, experimental details, gas sorption isotherms, DFT results, SEM-EDX and XPS data, NMR spectra, additional catalysis information, TGA and PXRD patterns, ICP-OES) and the ORCID identification number(s) for the author(s) of this article can be found under:
https://doi.org/10.1002/anie.201802402.

$CO_2H\}_3$; tctpH$_3$) and 4,4′-bipyridine (bipy) ligands to [M$_3$-(OH)]$^{5+}$ nodes (M = Co, Ni). Crystalline PCM-101 was obtained in high yields by slow heating of solutions of M(BF$_4$)$_2$ and the ligands at 75°C over 12 h, in DMF:MeOH:H$_2$O solvent (5:2:1). Single crystal X-ray diffraction (SCXRD) of the Co^{II} analogue gave the formula, [Co$_6$(μ_3-OH)$_2$(tctp)$_4$(4,4′-bipy)$_3$]·HBF$_4$·7H$_2$O·2H$_3$O·5DMF, in good agreement with all other characterizing data (Supporting Information). PCM-101 occupies the orthorhombic space group *Immm* (Z = 2); the Co and Ni analogues are isostructural and phase-pure, confirmed by powder X-ray diffraction (PXRD; Supporting Information, Figure S1). TctpH$_3$ is susceptible to slow oxidation; products obtained from reactions conducted in air using bench solvents result in some oxidation to P=O (between 10–25% by FTIR and SCXRD; Supporting Information, Figure S2). Reactions prepared under N$_2$ using degassed solvents provide oxide-free isolated crystalline products.

The high-symmetry [M$_3$(μ_3-OH)]$^{5+}$ clusters act as octahedral nodes, in which the three equatorial cluster sites are occupied by bipy-*N* donors (N1 and N2; Figure 1A); there is no coordinated solvent in the lattice. Calculated bond valence sum (BVS)[9] values using the Co-PCM-101 bond distances give average net charge values of −1.21 for the central μ_3-*O* atom and +2.06 for each Co^{II} ion. As observed previously,[8]

the trigonal tctp$^{3−}$ phosphine trianion favors the formation of 2D bilayer sheets with surfaces decorated with P: groups (Figure 1B,C). Importantly, the 2D bilayers in PCM-101 are fused into 3D arrays via 4,4′-bipy inter-layer pillars linking between adjacent [M$_3$(OH)]$^{5+}$ nodes (blue ligands; Figure 1); 4,4′-bipy ligands are also present as intra-layer pillars (green ligands; Figure 1). As a result, phosphine lone pairs on either side of a pore point directly at one another, with a P···P centroid separation of 7.22 Å, dictated by the inter-layer separation imposed by 4,4′-bipy. This arrangement provides accessible *trans*-bis(phosphine) coordination pockets. The largest pores have van der Waals-accessible openings of 11.7 × 22.9 Å (Figure 1C).

PCM-101 is thermally stable up to 340°C and solvent of crystallization is removed upon heating below 175°C (Supporting Information, Figure S3). The desolvated materials prepared using Co^{II} or Ni^{II} are permanently porous, confirmed by gas adsorption-desorption analysis of bulk samples (Supporting Information, Figures S4 and S5). The Ni^{II}-based material consistently formed in the highest yield, so it was used for subsequent bulk experiments. Gas sorption analysis using N$_2$ (78 K) and CO$_2$ (196 K) gave BET surface areas of 315 m^{2}g^{-1} and 350 m^{2}g^{-1}, respectively, with corresponding pore volumes of 0.17 and 0.19 cm^{3}g^{-1}. PCM-101 provides a unique platform to study post-synthetic metalation reactions at the *trans*-bis(phosphine) sites, in the solid-state because long-range order is maintained upon metalation, permitting full SCXRD analysis of the composite materials-examples of which remain rare amongst MOFs.

First, PCM-101 was treated with (dimethylsulfide)gold(I) chloride. (Me$_2$S)AuCl is a small precursor that is known to form simple, linear P−AuCl monophosphine coordination complexes;[10] SMe$_2$ is also a volatile ligand that is easily removed under vacuum. As-synthesized PCM-101 suspended in the mother liquor was directly treated with an equimolar solution of (Me$_2$S)AuCl and allowed to stand at room temperature for 12 h under N$_2$ without stirring. Bulk PXRD analysis of the products gave a very different pattern, indicating a change in metric symmetry (Supporting Information, Figure S6). SCXRD confirmed successful terminal coordination of AuCl to the P: sites, with a refined site occupancy of 55%. The single crystal-to-single crystal metalation incurred a large distortion of the host lattice, causing tilting of the pores in the crystallographic *ab* plane (Figure 2A(i)). The origin of the distortion is a change in the coordination bond angles subtended between the pillaring 4,4′-bipy-N2 and Co2 atoms from 180 to 169.7° (Figure 1A; compare Figure 2A(i)). This induces a lowering of cell symmetry such that AuCl-PCM-101 inhabits the primitive orthorhombic space group, *Pnnm* (Z = 4). The C−P−C bond angles also become slightly more obtuse upon AuCl coordination (from 102.5–103.0° to 102.3–107.4°).

The measured surface areas and pore volumes were moderately reduced upon addition of AuCl into the pores (S_{BET} = 282 and 181 m^{2}g^{-1}; V_{pore} = 0.14 and 0.08 cm^{3}g^{-1} for N$_2$ and CO$_2$, respectively; Supporting Information, Figure S7). 2D energy-dispersive X-ray (EDX) mapping of the crystallites conducted by scanning electron microscopy (SEM) confirmed uniform incorporation of Au^I throughout the crystallites
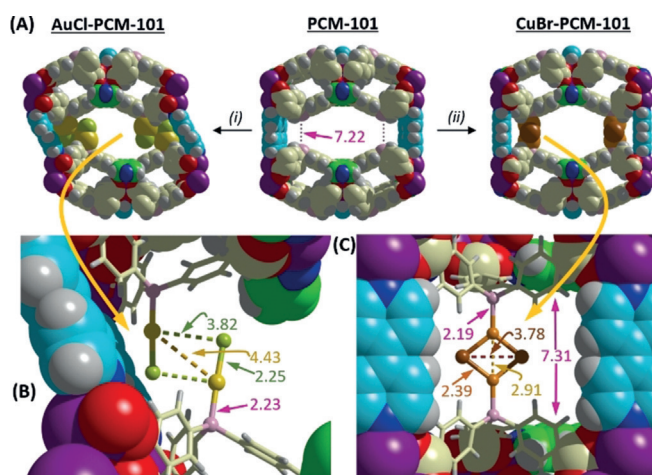
Figure 1. A) Expanded asymmetric unit of PCM-101 depicting one complete tctp$^{3−}$ group (yellow bonds) coordinated to three [Co$_3$(μ_3-OH)]$^{5+}$ nodes and two 4,4′-bipy ligands; blue = inter-layer pillaring ligands; green = intra-layer ligands bridging between adjacent metal nodes. B) Space-filling model of PCM-101 in the crystallographic *bc* plane showing square channels decorated with P: sites. C) Alternative view in the *ab* plane sowing the larger diamond-shaped pores with *trans*-oriented P: sites.[22]

Figure 2. A) Space-filling comparisons of the X-ray crystal structures of the parent PCM-101 (center) and the post-synthetically metalated materials: (i) 1 equiv (Me₂S)AuCl, 20°C, 12 h, 1 atm N₂; (ii) 1 equiv (Me₂S)CuBr; otherwise identical conditions to those in (i). B) Zoomed regions of the modified materials showing the phosphine–metal halide coordination geometries. All of the bond distances are shown in Angstroms, and dashed bonds show contact distances.[22]

(Supporting Information, Figure S8). There was no evidence of reduction to metallic Au in the EDX maps, XPS analysis or in the bulk PXRD pattern of AuCl-PCM-101 (Supporting Information, Figures S6, S8, S9). Bulk compositional analysis of AuCl-PCM-101 performed by inductively-coupled plasma-optical emission spectrometry (ICP-OES) indicated 63% Au occupancy (Supporting Information, Table S1).

This finding raises an important question, namely whether approximately half of the P₂ pockets are occupied by Au_2Cl_2 dimers, or whether isolated AuCl groups are the dominant species. Closer inspection of the single crystal structure of AuCl-PCM-101 provides a plausible answer to this question (Figure 2B): while the P–Au and Au–Cl bond distances are in-line with analogous molecular complexes,[10] the distances between Au and Cl centers in a putative dimer (Figure 2B; dashed bonds) are too long to constitute meaningful interactions. Aurophilic bonds fall within the range 2.7–3.5 Å,[11] but the Au sites in AuCl-PCM-101 are separated by 4.43 Å; similarly, the Au–Cl distances in bulk AuCl are 2.36 Å compared to 3.82 Å here.[12] Equally, coordination of an isolated AuCl moiety in the undistorted PCM-101 structure would leave a separation distance of only 3.17 Å between the Cl atom and uncoordinated P: site opposite it. In further support of this result, density-functional theory (DFT) was applied to the distorted AuCl-loaded structure and to the original (undistorted) PCM-101 structure loaded with dummy AuCl groups set to 50% occupancy, allowing only the AuCl groups to relax (Supporting Information, Figures S11, S12). In the actual distorted structure, clear separation of the electronic iso-surfaces between Cl and P atoms (4.22 Å) on opposite sides of the pore is achieved. In contrast, there is significant overlap between the electron clouds in the eclipsed structure. The calculated P–Au binding energies were −271.9 and −240.8 kJ mol⁻¹, respectively. Thus, the distortion is likely driven by sterics, allowing a single AuCl to be coordinated in a regular linear orientation at one of the two P: sites in every P₂ pocket.

To gain a better understanding of the AuCl loading mechanism in relation to the observed structural distortion, we performed a series of additional experiments using fractional amounts of the AuCl precursor. When PCM-101 was treated with 0.25 or 0.5 molar equiv of (Me₂S)AuCl, the bulk PXRD spectra resembled the unloaded parent PCM-101 material (Supporting Information, Figure S10). Interestingly, when 0.75 equiv were added, the PXRD pattern showed reflections corresponding to both the original *I*-centered cell and the distorted *P*-centered cell. This indicates that higher % Au loading is a driving force for the structural deformation.

We next attempted to achieve cooperative metalation using the *trans*-P₂ pockets in PCM-101. By performing a search of known *trans*-bis(phosphine) complexes in the Cambridge Structural Database (CSD), we noticed that the family of *trans*-$(R_3P)_2Cu_2Br_2$ dimers fall in the range 6.35–7.56 Å (mean = 7.31 Å),[13] encompassing the P···P separation distance in PCM-101 (7.22 Å). Direct treatment of PCM-101 with CuBr·MeSMe yielded single crystals that were visibly unchanged. SCXRD revealed the successful insertion of Cu_2Br_2 squares into P₂ pockets with retention of host lattice symmetry (Figure 2A(ii),C). The refined site occupancy of CuBr moieties in this material was 56% compared with 52% by ICP-OES analysis (Supporting Information, Table S1), indicating that slightly more than half of the available P₂ pockets were occupied with Cu_2Br_2 dimers. As for LAuCl complexes, monomeric CuBr-phosphine coordination complexes are linear, but rarely seen, requiring sterically encumbered phosphines such as P(Mes)₃.[14] Commonly, CuBr forms dimers and larger clusters (for example, $P_4Cu_4Br_4$)[15] with angular P–Cu–Br bonds, as observed here. Interestingly, CuBr incorporation into PCM-101 incurs a slight expansion of the *trans*-P···P distance from 7.22 to 7.31 Å for the framework to accommodate the Cu_2Br_2 moiety. Accordingly, the Cu_2Br_2 dimers are compressed along the P–Cu···Cu–P vector when compared to unsupported small molecule analogues in the CSD. This suggests that the MOF applies a steric pressure to the cluster. The Cu···Cu distance is 6% shorter than the observed mean value (2.91 Å; mean = 3.08 Å) while the Cu–Br distances (2.39 Å) are the shortest observed.[16]

Extensive solid-state characterization of CuBr-PCM-101 by SEM/EDX and PXRD confirmed clean and uniform incorporation of Cu^I throughout the crystals (Supporting Information, Figures S13, S14). Interestingly, while CuBr-PCM-101 showed an expected decrease in its BET surface area for CO₂ (223 m² g⁻¹), the BET surface area by N₂ was increased by 36% to 429 m² g⁻¹ (Supporting Information, Figure S15). This may be indicative of enhanced N₂ sorption at the accessible Cu_2Br_2 groups. Enhanced gas sorption by this material, and by other post-synthetically metalated versions of PCM-101, is presently under investigation in our laboratory.

To assess the accessibility and reactivity of metalated groups in the pores of PCM-101, catalytic alkyne hydroaddition was chosen as a model probe reaction (Scheme 1). This conversion is well understood in homogeneous systems, and is catalyzed by late transition-metal complexes,[17] including Cu^I and Au^I.[18] In this reaction, an alkyne feedstock (4-pentyn-1-ol, **1**; Scheme 1) is activated via coordination to the transition metal ion. Intramolecular nucleophilic attack by
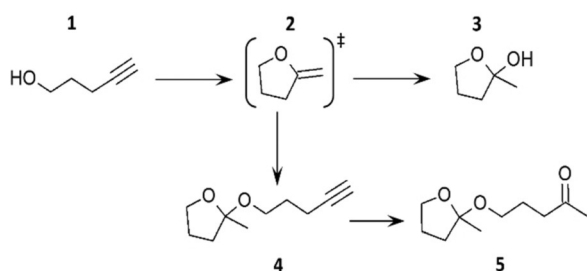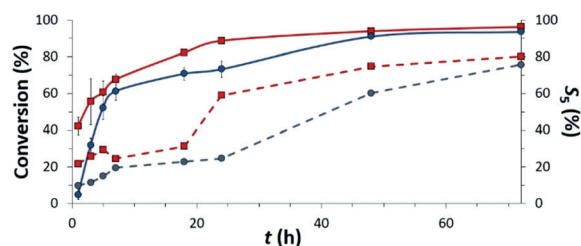
Scheme 1. M-PCM-101-catalyzed hydroaddition of 4-pentyn-1-ol (**1**) showing the expected alcohol **3**, and observed alkyne **4**, and ketone **5** obtained by condensation of intermediate **2** with a second equiv of the feedstock, **1**.

Figure 3. Time-dependent catalytic conversion (——) and selectivity (-----) for AuCl-PCM-101 (blue) and the ball-milled material (red).

Table 1: Data for the PCM-101-catalyzed intramolecular hydroaddition of 4-pentyn-1-ol after 24 h.

Entry	Catalyst[a,b]	Con. [%][c]	S_4 [%][c]	S_5 [%][c]
1	CuBr-PCM-101	22	86	14
2	AuCl-PCM-101	76	77	23
3	1st recycle	58	76	24
4	2nd recycle	34	83	17
5	3rd recycle	20	87	13
6	AuCl-PCM-101*	89	41	59
7	{(Ph₃P)CuBr}₂	4	94	6
8	(Ph₃P)AuCl	55	90	10
9	PCM-101	0	0	0

[a] See the Supporting Information. [b] 2.5 mol% catalyst loading in all cases. [c] determined by ^{1}H-NMR versus C_6H_6 internal standard. *Denotes the ball-milled catalyst.

the alcohol followed by proton transfer yields the *gem*-alkene, **2**, which quickly reacts with water to give the *hemi*-acetal, **3**.[19] Alternatively, nucleophilic attack at **2** by a second equiv of **1** gives the furan **4**; hydration of the alkyne in **4** yields the ketone **5** (Scheme 1).

This reaction was considered a useful model probe for the metallated PCM-101 materials for several reasons: the cyclized products are easily distinguished from the reactants by ^{1}H-NMR studies; the cyclic products have a larger critical diameter than the linear precursors, which could present mass-transport limitations inside the PCM-101 micropores, and the constrained reaction environments inside the micropores might result in differences in reaction orientations, leading to different product outcomes compared with solution-phase reactions. The Au^I-catalyzed hydroaddition of **1** to **3** was demonstrated by Mon et al.,[19] who employed a thioether-decorated methionine MOF as the catalyst support. They obtained **3** under mild conditions and without the need for activation of the S-AuCl sites with weakly coordinating anions. In our experiments, vacuum-dried M-PCM-101 crystals (M = CuBr, AuCl; 2.5 mol%) were suspended in dry CDCl₃, to which was added 1 equiv of **1** and an equimolar amount of C_6H_6 to act as an internal NMR standard.

The mixtures were sealed and left to react at 50°C. Aliquots were removed for analysis by ^{1}H-NMR at various times between 1–72 h (Figure 3; Supporting Information, Figures S16–S33; Table S3). Control reactions were also performed under identical conditions, using un-metalated PCM-101 and small molecule catalysts ([(Ph₃P)CuBr]₂[20] and (Ph₃P)AuCl;[10] Supporting Information, Figures S34, S35). The results obtained after 24 h are shown in Table 1.

A direct comparison of the data in Table 1 shows that the metalated PCMs were both significantly more active than their molecular counterparts under identical reaction conditions (entries 1 and 2 vs. 7 and 8). The AuCl-based material was much more active than the CuBr material, in line with the observed molecular reactivity. All reactions yielded exclusively the condensation products **4** and **5**. An un-metalated PCM-101 control showed no measurable activity (entry 9). After 24 h, the PCM catalysts yielded 14–25% of ketone **5**, obtained by hydration of **4**, which is known to be mediated by Au^I.[21] As the reaction progressed further, conversion of **4** to **5** increased to 80% (Figure 3; blue data). The increase in hydration products with time indicates that residual water was present inside the pores, even though pre-dried solvents were employed.

The post-catalysis AuCl-based materials were analyzed by PXRD, TGA, IR, TEM, and XPS (Supporting Information, Figures S36–S42). No evidence of reduction to Au^0 clusters or bulk metal was found in the PXRD pattern or by TEM imaging; XPS indicated the presence of ca. 6% Au^{III}, which is likely to correspond to molecular Au^{III} species generated by oxidative addition of alkynes to the Au^I centers. Au^{III} complexes have been shown to be active hydroaddition intermediates.[19] Recyclability studies of AuCl-PCM-101 showed that the material remained active after multiple reuses, although a continual reduction in catalytic activity was observed (Table 1; entries 2–5, and Supporting Information, Figures S43, S44). To further probe the potential cause of the observed loss of activity in AuCl-PCM-101 upon recycling, the material recovered after four cycles was analyzed by ICP-OES, which revealed a 10% decrease in total Au content compared to the fresh catalyst (from 63 to 53%; Supporting Information, Table S3).

Efforts were also made to assess whether the catalytic reactions were occurring predominantly at (or near) the crystallite surfaces, or inside the micropores. If the former were true, increasing the crystallite surface area-to-volume ratio should result in a proportional increase in the observed rate of catalysis. Samples of AuCl-PCM-101 were thus ground by ball mill to produce microcrystalline powders. SEM/EDX and PXRD analyses showed no formation of nanoparticles upon milling (Supporting Information, Figures S45, S46). SEM was used to measure the average change in surface area to volume ratio by assuming cubic morphology (Supporting Information, Figures S47, S48). The surface area-to-volume ratio of the ball-milled crystallites was increased by 3076% compared to the unground material. However, the observed conversion of the milled sample after 24 h was only increased

by 22% (Table 1; entries 2 and 6, and Figure 3; red data). Grinding should increase the number of accessible pore openings and decrease the average pore length, alleviating mass transport limitations. This may explain the modest increase in the rate of catalysis observed herein. In contrast, after grinding, the percentage of AuCl sites on the crystallite surfaces versus those inside the crystals is only increased from 0.013% to 0.42% (Supporting Information, Table S4). The overall conversions observed were similar to those obtained for equimolar amounts of the molecular catalyst, so it is highly likely that the catalysis occurred inside the pores in this study. XPS of the ball-milled materials post-catalysis also indicated a greater amount of Au^{III} than in the unground samples (Supporting Information, Figure S40).

In summary, we have demonstrated the post-synthetic metalation of a phosphine-based MOF, with full X-ray diffraction analysis of the resulting structures. The flexible nature of PCM-101 in the solid state allowed the incorporation of different Group 10 metal species via the formation of direct P−M bonds. These metal species are both stable with respect to leaching and are readily accessible, acting as single-site heterogeneous catalysts that show higher activity than their molecular counterparts.

Conflict of interest

The authors declare no conflict of interest.

[1] a) S. M. J. Rogge, et al., *Chem. Soc. Rev.* **2017**, *46*, 3134; b) T. Devic, C. Serre, *Chem. Soc. Rev.* **2014**, *43*, 6097; c) S. Yuan, L. Zou, H. Li, Y.-P. Chen, J. Qin, Q. Shang, W. Lu, M. B. Hall, H.-C. Zhou, *Angew. Chem. Int. Ed.* **2016**, *55*, 10776; *Angew. Chem.* **2016**, *128*, 10934; d) R. Ricco, C. Pfeiffer, K. Sumida, C. J. Sumby, P. Falcaro, S. Furukawa, N. R. Champness, C. J. Doonan, *CrystEngComm* **2016**, *18*, 6532.

[2] a) B. Chen, S. Xaing, G. Quain, *Acc. Chem. Res.* **2010**, *43*, 1115; b) Z. R. Herm, B. M. Wiers, J. A. Mason, J. M. van Baten, M. R. Hudson, P. Zajdel, C. M. Brown, N. Masciocchi, R. Krishna, J. R. Long, *Science* **2013**, *340*, 960.

[3] a) T. Sawano, Z. Lin, D. Boures, B. An, C. Wang, W. Lin, *J. Am. Chem. Soc.* **2016**, *138*, 9783; b) Y.-L. Hou, K.-K. Yee, Y.-L. Wong, M. Zha, J. He, M. Zeller, A. D. Hunter, K. Yang, Z. Xu, *J. Am. Chem. Soc.* **2016**, *138*, 14852; c) M. Mon, F. Loret, J. Ferrando-Soria, C. Marti-Gastaldo, D. Armentano, E. Pardo,

Angew. Chem. Int. Ed. **2016**, *55*, 11167; *Angew. Chem.* **2016**, *128*, 11333; d) F. R. Fortea-Perez, et al., *Nat. Mater.* **2017**, *16*, 760.

[4] a) S. S. Y. Chui, S. M. F. Lo, J. P. H. Charmant, A. G. Orpen, I. D. Willaims, *Science* **1999**, *283*, 1148; b) Y. K. Hwang, D.-Y. Hong, J.-S. Chang, S. H. Jhung, Y.-K. Seo, J. Kim, A. Vimont, M. Daturi, C. Serre, G. Férey, *Angew. Chem. Int. Ed.* **2008**, *47*, 4144; *Angew. Chem.* **2008**, *120*, 4212; c) C. P. Krap, et al., *Inorg. Chem.* **2016**, *55*, 1076.

[5] a) A. J. Nuñez, L. N. Shear, N. Dahal, I. A. Ibarra, J. Yoon, Y. K. Hwang, J.-S. Chang, S. M. Humphrey, *Chem. Commun.* **2011**, *47*, 11855; b) A. J. Nuñez, M. S. Chang, I. A. Ibarra, S. M. Humphrey, *Inorg. Chem.* **2014**, *53*, 16038; c) X. Yu, S. M. Cohen, *J. Am. Chem. Soc.* **2016**, *138*, 12320; d) W. M. Bloch, A. Burgun, C. J. Coghlan, R. Lee, M. L. Coote, C. J. Doonan, C. J. Sumby, *Nat. Chem.* **2014**, *6*, 906.

[6] a) A. M. Bohnsack, I. A. Ibarra, V. I. Bakhmutov, V. M. Lynch, S. M. Humphrey, *J. Am. Chem. Soc.* **2013**, *135*, 16038; b) J. He, N. W. Waggoner, S. G. Dunning, A. Steiner, V. M. Lynch, S. M. Humphrey, *Angew. Chem. Int. Ed.* **2016**, *55*, 12351; *Angew. Chem.* **2016**, *128*, 12539; c) J. He, A. M. Bohnsack, N. W. Waggoner, S. G. Dunning, V. M. Lynch, W. C. Kaska, S. M. Humphrey, *Polyhedron* **2018**, *143*, 149.

[7] J. F. Hartwig, *Organotransition Metal Chemistry—From Bonding to Catalysis*, University Science Books, New York, **2010**.

[8] S. M. Humphrey, P. K. Allan, S. E. Oungoulian, M. S. Ironside, E. R. Wise, *Dalton Trans.* **2009**, 2298.

[9] I. D. Brown, *The Chemical Bond in Inorganic Chemistry: The Bond Valence Model*, Oxford Univ. Press, Oxford, **2002**.

[10] a) G. E. Coates, C. Parkin, *J. Chem. Soc.* **1963**, 421; b) L. Malatesta, L. Naldini, G. Simonetta, F. Cariati, *Coord. Chem. Rev.* **1966**, *1*, 255.

[11] H. Schmidbaur, *Gold Bull.* **2000**, *33*, 3.

[12] E. M. W. Janssen, J. C. W. Folmer, G. A. Wiegers, *J. Less-Common Met.* **1974**, *38*, 71.

[13] CSD Refcodes: EVOPUC, EVOPUC02, HABKIH, IGEKAG, LEJYAA, NAFPAM, OFUTEO, PAWBAR, PECHUA, PECHUA01, PECHUA02, QABZUO, VUHYIG, VUHZAZ.

[14] E. C. Alyea, G. Ferguson, J. Malito, B. Ruhl, *Inorg. Chem.* **1985**, *24*, 3719.

[15] a) R. G. Goel, A. L. Beauchamp, *Inorg. Chem.* **1983**, *22*, 395; b) P. F. Barron, J. C. Dyason, L. M. Engelhardt, P. C. Healy, A. H. White, *Inorg. Chem.* **1984**, *23*, 3766.

[16] S. Krupski, G. Kehr, C. G. Daniliuc, G. Erker, *Dalton Trans.* **2016**, *45*, 6111.

[17] a) S. Elgafi, L. D. Field, B. A. Messerle, *J. Organomet. Chem.* **2000**, *607*, 97; b) B. A. Messerle, K. Q. Vuong, *Organometallics* **2007**, *26*, 3031.

[18] a) M. F. N. N. Carvalho, T. A. Fernandes, A. M. Galvão, H.-A. K. von Nidda, M. A. P. Sampai, *Inorg. Chim. Acta* **2010**, *363*, 1767; b) A. Zhdanko, M. E. Maier, *Chem. Eur. J.* **2014**, *20*, 1918.

[19] M. Mon, J. Ferrando-Soria, T. Grancha, F. R. Fortea-Pérez, J. Gascon, A. Leyva-Pérez, D. Armentano, E. Pardo, *J. Am. Chem. Soc.* **2016**, *138*, 7864.

[20] J.-L. Chen, X.-Z. Tan, X.-F. Fu, X.-X. Chen, J.-Y. Wang, L.-H. He, H.-R. Wen, *J. Coord. Chem.* **2014**, *67*, 1186.

[21] a) C. Khin, A. S. K. Hashmi, F. Rominger, *Eur. J. Inorg. Chem.* **2010**, 1063; b) S. G. Weber, D. Zahner, F. Rominger, B. F. Straub, *ChemCatChem* **2013**, *5*, 2330.

[22] CCDC 1581200, 1581201, 1581202, and 1581203 contain the supplementary crystallographic data for this paper. These data are provided free of charge by The Cambridge Crystallographic Data Centre.